

12

Chemical Modelling of EC2

12.1 Method

To investigate the properties of EC2 and to see whether it is typical of material which has been less processed, a chemical kinetic model was made using my observationally derived temperatures and densities, varying elemental abundances, photon fluxes, cosmic ray ionisation (CRI) rates and gas-to-dust ratios in an attempt to fit my observed results. The model is based on the HMC code by Rodgers (1998), which utilises the Livermore Solver for Ordinary Differential Equations (Hindmarsh 1983; Radhakrishnan and Hindmarsh 1993). Chemical reaction rates were taken from Rate99: The UMIST database for astrochemistry (Le Teuff et al. 2000). To compare model results with my observations I adapted Perl scripts created by Roberts (2006) to generate Tables 12.1-12.5 and the data for the plots in Figs. 12.1-12.15.

The basic model assumes $T_{\text{kin}} = 20 \text{ K}$, $n(\text{H}_2) = 1.2 \times 10^4 \text{ cm}^{-3}$, based on my NH_3 , H_2CO , and CO observations, and uses the initial elemental abundances as listed in Table 12.6 which, for metals C, N, O, S, Si and Fe are reduced by a factor of five from those typically used for local ISM clouds; I find that without this reduction in elemental abundances, agreement with observations is worsened for $A_V > 1 \text{ mag}$. I have investigated varying the CRI rate and the visual extinction (A_V) in order to try

12: CHEMICAL MODELLING OF EC2

and find the best fit to the observations. I also varied the UV photon field, initial abundances, and specifically the abundances of sulphur or nitrogen. At a distance of 20 kpc, a 60'' beam subtends a linear distance of about 6 pc or a column density of about $2 \times 10^{23} \text{ cm}^{-2}$ for $n(\text{H}_2) = 1.2 \times 10^4 \text{ cm}^{-3}$. Since my CO maps show that EC2 is extended and clumpy, the ‘one-point’ model adopted is simplistic; nevertheless, given the lack of data on very small scales, one might hope that the model helps constrain some of the global parameters in the cloud in a ‘beam-averaged’ sense. 321 models with varying parameters were run, and the detailed results of testing each one against my observations are listed in Appendix O.

To test the agreement between each model and my observations, I looked at the ratio of the observed abundance relative to H_2 from Table 9.3 to the model prediction (or the inverse of that ratio if it was greater than 1) for that species. In the case of my multiple transition detections of ^{12}CO , ^{13}CO and C^{18}O , I have used a σ weighted mean of each isotopomer’s observed column densities, where $\sigma = T_{\text{mb}}/r\text{ms}_{\text{mb}}$. However, as the models only consider the main isotope of an atom (with the exception of H and D) I have assumed that the isotopic ratios have their local interstellar values ($^{12}\text{C}/^{13}\text{C} = 60$, $\text{C}^{16}\text{O}/\text{C}^{18}\text{O} = 500$), and factored my observed (mean) abundances relative to $N(\text{H}_2)$ accordingly. For the ^{13}CO and C^{18}O transitions, this gives me a reasonably consistent value of $N(\text{CO})/N(\text{H}_2) \sim 10^{-6}$, although the main ^{12}CO lines give a value closer to 10^{-7} . Since the main lines of ^{12}CO are assumed to be optically thick, the ratios derived from observation are lower limits. For each molecule/transition I then multiply the square of its agreement factor by its weight (see below), sum them for each model, then normalise to get a number between 0 and 1 that should be closest to 1 for the model which agrees best.

The tests were initially run with a weighting factor of unity for all species. I also examined the effect of applying a differential weighting factor for each molecule/transition, depending on how well determined I thought its abundance might be: NH_3 and H_2CO a weight of 4, due to the hyperfine fitting that was able to be done; C also a weight of 4, due to my JCMT detection and because it is quite sensitive to the model

parameters; C₂H a weight of 3, as its abundance might be more sensitive to the model parameters; CN, DCO⁺, HCN, HNC, as well as C¹⁸O and ¹³CO, a weight of 2; and the remaining species, including ¹²CO, unit weight. I also considered how well the model agreed with the fractional abundance of CO, and based on the LVG modelling (see section 9.4), which took the optical depth (τ in Table 9.4) of each isotopomer of CO into account, applied an alternative weighting scheme where each isotopomer of CO was given an equal weight of unity. The test of agreement between each model and my observations was therefore run for three different weighting schemes:

All=1 All weighting factors = 1;

CO=111 Differential weighting factors with ¹²CO/¹³CO/C¹⁸O = 1/1/1;

CO=122 Differential weighting factors with ¹²CO/¹³CO/C¹⁸O = 1/2/2.

In Appendix O, Fig. O.1 compares the effect of the three weighting schemes described above, and Tables O.1-O.6 list the agreement fit results for each model for each of the three weighting regimes. It can be seen that the highest agreement factor (or fit) is achieved when *all* weighting factors are unity (*All=1*), and that apart from a flattening of the fit between $A_V = 0.5-1.0$ mag for high CRI, UV or initial abundances, the general trends are the same for all three weighting schemes, with the *CO=122* regime producing the lowest fit scores, but only slightly lower than those for the *CO=111* regime. I conclude that the test of agreement between each model and my observations is most effective without weighting, and therefore present the non-weighted results below.

12.2 Results

I have selected 16 models for detailed examination, and they can be compared in Tables 12.1 to 12.5. A comparison of the agreement factor varying over time for these models can be seen in Figs. 12.1 to 12.5. Figs. 12.6 to 12.10 show fractional abundances varying over time for five of the 16 models. I also investigated the agreement factor

at steady-state ($t > 10^6$ yr), and Figs. 12.11 through 12.15 plot 3D parameter surfaces of these test results for various combinations of the models, where two parameters are varied and the others are kept constant. For ease of comparison, numbered blue disks, marked on the 3D plots, indicate the 16 examined models relative to the parameter surfaces.

Varying CRI and A_V

I investigated the agreement tests for values of A_V between 0.5 and 10 mag, and a CRI rate between 0.5 and 30 times the standard interstellar rate of $1.3 \times 10^{-17} \text{ s}^{-1}$, with $T = 20 \text{ K}$, $n(\text{H}_2) = 1.2 \times 10^4 \text{ cm}^{-3}$, a UV field set to the local ISM value, and most initial abundances reduced by a factor of 5 from typical local values (see Table 12.6). Although many of the models give very similar results, the agreement factor is highest for a CRI rate above $10 \times$ the ISM value and an A_V of 1 mag. Figure 12.11 shows the general trend of varying A_V and CRI, and it can be seen that increasing the CRI rate beyond $20 \times$ the ISM value extends agreement in the model to $A_V = 2$ mag. What is striking however, is the failure of the model for values of A_V above 2 mag. It should be noted that model results for $A_V \leq 0.5$ mag should be treated with caution, as the model may fail for such low values of A_V , since it does not treat the self-shielding of H_2 and CO accurately for very low A_V .

Table 12.1 shows how well these models actually agree with the observations for four selected models (1–4). Model 1 uses ‘standard’ ISM values for the A_V and CRI rate, Model 2 is the best fit model (CRI = $2.6 \times 10^{-16} \text{ s}^{-1}$, $A_V = 1$ mag), while Model 3 uses CRI = $1.3 \times 10^{-16} \text{ s}^{-1}$ and $A_V = 2$ mag, just to illustrate some effects which arise from changing these parameters. Model 4 is the same as Model 3, but with a UV field 10 times the local rate.

For Model 1 the predicted CO/ H_2 ratio is 1 or 2 orders of magnitude higher than all the observations. Models 2 and 4 agree within a factor of 2 for ^{12}CO but underestimate ^{13}CO and C^{18}O by ~ 1 order of magnitude, whereas Model 3 reverses those

agreements. Looking at the steady-state fractional abundances of CO predicted by the models, Model 1 gives 2.9×10^{-5} , Model 3 gives 2.2×10^{-6} , while Models 2 and 4 give 2.5×10^{-7} and 2.3×10^{-7} , respectively, agreeing very well with observation.

Model 1 does badly at reproducing the observed value for atomic C, since when the A_V is 10 mag the cloud is shielded from UV radiation and the bulk of the carbon becomes incorporated into CO. When the A_V is lowered and/or the CRI rate increased, however, CO can be broken down, so that the abundance of C I remains significant even at steady-state. I find that an A_V of 1 or 2 mag gives a better agreement with the EC2 observation of $N(\text{C})/N(\text{H}_2)$.

The predicted value of $\text{C}_2\text{H}/\text{H}_2$ in Model 1 agrees with the observations to within a factor of 2, while the other three Models are 10 to 40 times too high. Conversely, Models 1 and 3 over-predict the CN/H_2 ratio by over 2 orders of magnitude, with Models 2 and 4 over-estimating by 40 and 50 times respectively.

Of course, all these models are at steady-state after a million years, but I can look at how the agreement factor changes over time: Fig. 12.1 shows that both Model 2 and 4 have good agreement from the earliest times ($t = 2 \times 10^3$ yr), whereas neither Model 1 or 3 show good agreement beyond the first 500 years.

Varying UV photon field, CRI and A_V

I have also looked at the effect of varying the photon field in the models. Fig. 12.12 shows agreement factors for models with varying A_V and CRI for (a) a UV field increased by a factor of 10 compared to the local ISM value, and (b) a UV field reduced by a factor of 10. It can be seen that a higher UV field improves agreement up to an A_V of 2 mag regardless of CRI rate (although for CRI $20 \times$ this is extended to 3 mag), with Model 4 (Table 12.1) the best fit. A lower UV field produces very poor agreement (e.g. Model 5).

Figure 12.13a plots fit results from models where the CRI rate is fixed at 20 times the standard value, A_V is varied, and the UV field is varied from one-tenth to 80 times

the local interstellar field. As expected, an increase in the UV photon field extends agreement to higher values of A_V (4 mag for $80 \times$ UV). Table 12.2 shows the agreement for four of these models, including my best-fit Model 2. Interestingly, $20 \times$ UV produces a good fit for atomic carbon at an A_V of 1 mag (Model 6), whereas $40 \times$ UV at an A_V of 3 mag gives a good fit for CO (Model 7). At steady-state CO is primarily destroyed by photons (only if the UV field is strong enough, or the A_V low enough) or by He^+ and H_3^+ , whose abundances increase with increasing CRI rate. Again a UV field below the local value produces very poor general agreement, but apart from very high UV fields ($\sim 70 \times$) at an A_V of ~ 4 mag, there is poor agreement for any A_V above 3 mag. Figure 12.2 shows how the agreement factor for Models 2 and 5–7 varies over time, and interestingly the high UV ($20 \times$) Model 6 shows remarkable agreement from the earliest times, and Model 7 ($40 \times$ UV) agrees well from $t = 2 \times 10^4$ yr.

The predicted $\text{DCO}^+/\text{HCO}^+$ ratio is around an order of magnitude too small for Model 5, whereas models 2, 6 and 7 underestimate by 2 orders. Cosmic ray ionisation of H_2 and He produce electrons which can destroy H_3^+ before it can react with HD, the initial step to deuterating most molecular ions. In models with enhanced CRI rates, the electron abundances are high ($8\text{--}9 \times 10^{-6}$, although the dominant ion is C^+ , which is normally produced by photons) and the predicted DCO^+ fractionation is very low.

For $\text{C}_2\text{H}/\text{H}_2$ and CN/H_2 , the ratios are overestimated by 2 orders of magnitude in the low UV Model 5, but the fit improves with increasing UV field, with good agreement reached at $20 \times$ UV (Model 6). Finally, I note that there is a much better fit to the ammonia abundance in low UV Model 5 (which is also achieved for NH_3 in Model 3 with $\text{UV} = 1$ and $\text{CRI} = 10$ times the local ISM rates).

Varying initial abundances and A_V

Initial elemental abundances (see Table 12.6) were varied between local ISM values and 10 per cent of those values, and the parameter surface in Fig. 12.13b shows that for A_V above 1 mag, the agreement worsens appreciably for initial abundances (IA) above

20 per cent of local cloud values. Table 12.3 compares Model 2 with Models 8–10, and for $IA = 0.1$ (Model 8) there is good agreement, except for atomic C and CN (~ 1 order of magnitude to great), NH_3 (~ 1 order to little), and SO (underestimated by 5 orders). Fig. 12.3 suggests that Model 8's agreement varies considerably in the first 10,000 years or so, before settling down at a steady-state below Model 2 ($IA = 0.2$).

Increasing initial abundance of sulphur

The observed $CS(2-1)/H_2$ ratio is fairly well matched by my best fit Models 2 and 4, and very well matched by Models 7 and 8 ($UV = 40$ and $IA = 0.1$ respectively), but except for Model 1, the predictions for SO are far too low by several orders of magnitude. Models 11–13 in Table 12.4 show the effect of increasing the initial abundance of sulphur relative to other initial abundances (which are set at 20 per cent of local cloud values). For CS the agreement deteriorates to an overestimation by 2 orders of magnitude for an initial $x(S)$ abundance 10 times the adopted local ISM value (Model 13), whereas in SO the underestimation by over 6 orders of magnitude in Model 2, is reduced to a little over 4 orders in Model 13. Fig. 12.15a shows little general improvement for Models 11–13 over Model 2, except that for $x(S)$ one order higher than the local ISM value, there is better general agreement up to $A_V \sim 4$ mag. Fig. 12.4 shows that just increasing initial $x(S)$ makes little difference to the agreement trend over time, although Model 13 agrees less well most of the time. Overall, it can be seen that abundances of sulphur bearing molecules scale linearly with any change in the initial abundance of S.

Depleting initial abundance of nitrogen

For the N-bearing species, all models (except 1, 3 and 5) give good agreement for HC_3N and N_2H^+ , but these detections are upper limits, so this result must be treated with some caution. For HCN and HNC the picture is less clear, but abundances are again well matched for my best fit Models 2 and 4. Models 3 and 5 are in good

12: CHEMICAL MODELLING OF EC2

agreement with the NH_3/H_2 ratio, while all other models (except Model 1) predict ratios 2 to 5 orders of magnitude too low. For CN the high UV Model 6 agrees with the observed abundance. Models 14–16 in Table 12.5 show the effect of further depleting the initial abundance of nitrogen relative to other initial abundances, which are set at 20 per cent of local values. For CN the agreement is improved to a reasonable fit for the highest N depletion in Model 16, but for HCN and HNC there is a slight improvement in agreement for Model 14, where $x(\text{N})$ is 10 per cent of the local value. However, for NH_3 the agreement gets worse by 2 to 4 orders of magnitude. Fig. 12.15b shows little general improvement for Models 14–16 over Model 2, and that regardless of the initial $x(\text{N})$ abundance, models with an A_V higher than 2 mag agree poorly. Fig. 12.5 shows that depleting the initial $x(\text{N})$ abundance makes little difference to the agreement trend over time, although the agreement for Model 14 between 1,000 and 5,000 years is markedly improved compared to the other models. As for sulphur, changing the initial abundance of N just scales the abundances of nitrogen bearing molecules at steady-state.

Varying $n(\text{H}_2)$ and A_V

Fig. 12.14 shows the effect of varying $n(\text{H}_2)$ (cm^{-3}) and A_V (mag) with (a) a UV field set to the local ISM value, and (b) a UV field increased by a factor of 10. The CRI rate is 20 times the local ISM value and most initial abundances are reduced by a factor of 5. It can be seen that densities above $n(\text{H}_2) = 1.2 \times 10^4 \text{ cm}^{-3}$ produce a marked falloff in agreement, and that even for a UV field 10 times the local interstellar value, the visual extinction must be below $A_V = 3$ mag for reasonable agreement.

Deuteration

I failed to detect any deuterated species in this survey, with the upper limits being: $\text{DCO}^+/\text{HCO}^+ < 0.08$; $\text{DCN}/\text{HCN} < 1.5$; $\text{C}_2\text{D}/\text{C}_2\text{H} < 0.06$ and $\text{HDCO}/\text{H}_2\text{CO} < 0.01$. The models presented here use the underlying D/H ratio from the local ISM. Model 1

predicts $\text{DCO}^+/\text{HCO}^+ \sim 0.25$, which is higher than that seen in local dark clouds such as TMC-1 because of the lower abundance of heavy elements. Models 2 and 4, however, predict very low $\text{DCO}^+/\text{HCO}^+$ ratios ($\sim 10^{-3}$), whereas Model 3 predicts $\sim 10^{-2}$. The large upper limits on DCN/HCN and $\text{C}_2\text{D}/\text{C}_2\text{H}$ mean that these are not useful in constraining the models. Likewise for HDCO and DCO^+ the fractionation ratios agree except for Model 1.

12.3 Fractional abundances over time

In Figs. 12.6 through 12.10 I have plotted the fractional abundances varying over time for the best fit Models 2, 4, 6, 7 and 8, where $n(\text{H}_2) = 1.2 \times 10^4 \text{ cm}^{-3}$ and $T = 20 \text{ K}$.

Model 2: $A_V = 1 \text{ mag}$, $\text{CRI} = 20 \times$, $\text{UV} = 1 \times$, $\text{IA} = 0.2 \times$

For Model 2 it can be seen that steady-state is reached very quickly after around 5,000 years (apart from some slight changes in HCN and HCO^+).

Model 4: $A_V = 2 \text{ mag}$, $\text{CRI} = 10 \times$, $\text{UV} = 10 \times$, $\text{IA} = 0.2 \times$

Model 4 looks much like Model 2, with steady-state at $\sim 5,000 \text{ yr}$, although there is less CS , which fits observations better. As mentioned in section 12.2, a higher UV photon field improves agreement regardless of CRI rate.

Model 6: $A_V = 1 \text{ mag}$, $\text{CRI} = 20 \times$, $\text{UV} = 20 \times$, $\text{IA} = 0.2 \times$

The high UV photon field in Model 6 produces a photodissociation rate $20 \times$ that of Model 2, which shortens the time scale by $20 \times$, with steady-state reached at just $\sim 500 \text{ yr}$, but with more C^+ coupled to lower abundances of all other species.

Model 7: $A_V = 3$ mag, CRI = 20 \times , UV = 40 \times , IA = 0.2 \times

Although the very high UV photon field (40 \times) in Model 7 produces a good fit for higher extinction ($A_V = 3$ mag), steady-state is not reached until 10^4 yr, with some molecular abundances reaching a peak at $\sim 10^3$ yr (e.g. C_2H , CN and CS), before depleting slightly by steady-state. At steady-state, compared to Model 2, C and NH_3 abundances are higher, but C^+ , CS and C_2H are lower.

Model 8: $A_V = 2$ mag, CRI = 20 \times , UV = 1 \times , IA = 0.1 \times

With initial abundances set at 10 per cent of typical local ISM values, many of the abundances in Model 8 reach a peak at 10^4 yr before settling down to lower values at steady-state at 5×10^4 yr. Compared to Model 2, there is a higher abundance of NH_3 (although still an order of magnitude less than observed in EC2) and slightly more SO, with less CN, CS, C_2H , and a lot less C^+ . The trends in Model 8 look more like a typical dense cloud as opposed to diffuse or translucent clouds (which EC2 appears to be more like).

Are short timescales reasonable?

For cold, dense clouds (e.g. TMC-1) large abundances of NH_3 and SO indicate that chemical evolution is highly evolved, where it takes $\sim 10^6$ yr for NH_3 and SO in the cloud to reach steady-state. However, my models show that steady-state is reached much earlier ($\sim 10^4$ yr), so that there is ‘no difference’ between steady-state and early time. This early time is so short as to be ‘unphysical’, if EC2 is considered to be a standard molecular cloud with a lifetime well in excess of 10^6 yr. However, if the formation of EC2 has been triggered by some recent process, e.g. a supernova shock, then the time since its formation could be relatively short, justifying an observation of gas that is $\sim 10^4$ yr old.

Sulphur chemistry is also difficult to model, as although S is very reactive, the reaction rates for $CS + O$ and $SO + C$ (that allow $CS \leftrightarrow SO$) are not well defined, due

to a lack of knowledge of important low temperature neutral-neutral rate coefficients (Millar and Herbst 1990). The rate coefficient used for the $\text{SO} + \text{C} \rightarrow \text{CS} + \text{O}$ reaction is $1.70 \times 10^{-10} \text{ cm}^3 \text{ s}^{-1}$ (around twice that for $\text{SO} + \text{C} \rightarrow \text{CO} + \text{S}$), with the temperature sensitive reverse reaction effectively zero at 20 K, thus favouring the creation of CS. This is reflected in all models (except Model 1) failing to reproduce the observation that $\text{SO} \sim \text{CS}$. A much lower rate coefficient for $\text{SO} + \text{C} \rightarrow \text{CS} + \text{O}$ would reduce the destruction of SO to better fit observations.

The formation of ammonia is also difficult to model, as its abundance only builds up at later times in a molecular cloud's chemical evolution. This is because the proton affinity (PA) for N is less than that for H_2 , whereas for O, CO, S, N_2 , CH_3OH , $\text{PA}(\text{X}) > \text{PA}(\text{H}_2)$. Therefore, H_3^+ will not react with N, thus preventing a chain of reactions that could lead to the formation of NH_3 . Instead, ammonia is formed by slow endothermic reactions that start with $\text{N} + \text{OH}$ (although N more readily reacts with CH and CH_2 to form CN and HCN), or $\text{N}^+ + \text{H}_2$, where $n(\text{N}^+)$ is low because CRI is relatively inefficient.

12: CHEMICAL MODELLING OF EC2

Table 12.1: Comparison of observations of Edge Cloud 2 (EC2) with four different model predictions at steady-state. Abundances given relative to $N(\text{H}_2) = 7.4 \times 10^{22} \text{ cm}^{-2}$, with $n(\text{H}_2) = 1.2 \times 10^4 \text{ cm}^{-3}$ and $T = 20 \text{ K}$. Most model initial abundances relative to H reduced by a factor of 5 from typical local ISM values. Bold type indicates agreement to within a factor of 5.

Species	Observed in EC2	Model 1	Model 2	Model 3	Model 4
		$A_V = 10 \text{ mag}$ CRI = 1 \times UV = 1 \times	$A_V = 1 \text{ mag}$ CRI = 20 \times UV = 1 \times	$A_V = 2 \text{ mag}$ CRI = 10 \times UV = 1 \times	$A_V = 2 \text{ mag}$ CRI = 10 \times UV = 10 \times
^{13}CO	1.45e-06	2.90e-05	2.51e-07	2.22e-06	2.28e-07
C	1.04e-06	1.41e-08	1.37e-05	2.47e-05	1.79e-05
C^{18}O	1.36e-06	2.90e-05	2.51e-07	2.22e-06	2.28e-07
C_2D	<4.49e-11	1.14e-10	1.48e-11	6.70e-11	1.18e-11
C_2H	6.96e-10	1.65e-09	1.71e-08	2.79e-08	1.04e-08
CN	3.09e-11	7.61e-09	1.24e-09	6.82e-09	1.51e-09
CO	1.22e-07	2.90e-05	2.51e-07	2.22e-06	2.28e-07
CS (2–1)	4.57e-11	6.97e-09	2.87e-10	2.11e-09	1.46e-10
CS (3–2)	5.07e-12	6.97e-09	2.87e-10	2.11e-09	1.46e-10
DCN	<2.23e-11	9.37e-10	1.24e-14	2.98e-13	2.08e-14
DCO^+	<1.58e-12	1.78e-09	6.16e-15	5.12e-13	7.53e-15
H^{13}CN	<8.35e-11	6.13e-09	1.07e-11	1.28e-10	1.36e-11
H^{13}CO^+	<6.71e-11	7.26e-09	6.60e-12	5.36e-11	5.16e-12
H_2CO	7.58e-11	1.60e-08	7.70e-11	1.19e-09	9.38e-11
HC_3N	<3.54e-12	1.55e-10	7.26e-13	1.19e-11	2.57e-13
HCN	1.49e-11	6.13e-09	1.07e-11	1.28e-10	1.36e-11
HCO^+	1.96e-11	7.26e-09	6.60e-12	5.36e-11	5.16e-12
HDCO	<8.70e-13	4.08e-09	2.68e-13	2.59e-11	4.44e-13
HNC	4.70e-12	1.58e-08	2.09e-11	4.05e-10	2.48e-11
N_2H^+	<1.31e-12	4.21e-10	1.88e-14	1.55e-12	4.75e-14
NH_3	7.80e-11	1.21e-07	2.02e-13	5.14e-11	3.04e-13
SO	1.34e-10	7.16e-09	6.43e-16	1.47e-14	6.16e-16

Notes for Tables 12.1 through 12.5: Models only consider main isotopes (with the exception of H and D), so for ^{13}CO , H^{13}CN and H^{13}CO^+ , models are compared to observed abundances $\times 60$; and for C^{18}O , models are compared to observed abundance $\times 500$. For multiple transition detections of ^{12}CO , ^{13}CO and C^{18}O , a σ weighted mean of each isotopomer's observed column density is used, where $\sigma = T_{\text{mb}}/r_{\text{ms,mb}}$.

Table 12.2: Comparison of observations of Edge Cloud 2 (EC2) with four different model predictions at steady-state, but with varying UV field. Abundances given relative to $N(\text{H}_2) = 7.4 \times 10^{22} \text{ cm}^{-2}$, with $n(\text{H}_2) = 1.2 \times 10^4 \text{ cm}^{-3}$ and $T = 20 \text{ K}$. Most model initial abundances relative to H reduced by a factor of 5 from typical local ISM values. Bold type indicates agreement to within a factor of 5.

Species	Observed in EC2	Model 5 $A_V = 1 \text{ mag}$ CRI = 20 \times UV = 0.1 \times	Model 2 $A_V = 1 \text{ mag}$ CRI = 20 \times UV = 1 \times	Model 6 $A_V = 1 \text{ mag}$ CRI = 20 \times UV = 20 \times	Model 7 $A_V = 3 \text{ mag}$ CRI = 20 \times UV = 40 \times
^{13}CO	1.45e-06	2.79e-06	2.51e-07	6.66e-09	3.39e-07
C	1.04e-06	2.23e-05	1.37e-05	1.55e-06	2.50e-05
C^{18}O	1.36e-06	2.79e-06	2.51e-07	6.66e-09	3.39e-07
C_2D	<4.49e-11	1.17e-10	1.48e-11	1.03e-12	5.90e-12
C_2H	6.96e-10	6.97e-08	1.71e-08	1.34e-09	3.90e-09
CN	3.09e-11	1.24e-08	1.24e-09	3.98e-11	8.46e-10
CO	1.22e-07	2.79e-06	2.51e-07	6.66e-09	3.39e-07
CS (2–1)	4.57e-11	7.17e-09	2.87e-10	3.30e-12	5.92e-11
CS (3–2)	5.07e-12	7.17e-09	2.87e-10	3.30e-12	5.92e-11
DCN	<2.23e-11	4.51e-13	1.24e-14	2.27e-15	1.13e-14
DCO^+	<1.58e-12	6.42e-13	6.16e-15	8.48e-16	1.86e-14
H^{13}CN	<8.35e-11	2.44e-10	1.07e-11	2.13e-12	7.56e-12
H^{13}CO^+	<6.71e-11	8.63e-11	6.60e-12	1.13e-12	9.94e-12
H_2CO	7.58e-11	1.14e-09	7.70e-11	4.09e-12	8.30e-11
HC_3N	<3.54e-12	5.24e-11	7.26e-13	1.00e-15	1.09e-13
HCN	1.49e-11	2.44e-10	1.07e-11	2.13e-12	7.56e-12
HCO^+	1.96e-11	8.63e-11	6.60e-12	1.13e-12	9.94e-12
HDCO	<8.70e-13	1.98e-11	2.68e-13	8.56e-15	6.28e-13
HNC	4.70e-12	5.57e-10	2.09e-11	2.78e-12	3.68e-11
N_2H^+	<1.31e-12	1.92e-12	1.88e-14	2.87e-17	6.52e-14
NH_3	7.80e-11	6.18e-11	2.02e-13	3.83e-15	1.35e-12
SO	1.34e-10	2.96e-14	6.43e-16	1.56e-17	9.25e-16

12: CHEMICAL MODELLING OF EC2

Table 12.3: Comparison of observations of Edge Cloud 2 (EC2) with four different model predictions at steady-state, but with varying initial abundances. Abundances given relative to $N(\text{H}_2) = 7.4 \times 10^{22} \text{ cm}^{-2}$, with $n(\text{H}_2) = 1.2 \times 10^4 \text{ cm}^{-3}$ and $T = 20 \text{ K}$. Most model initial abundances relative to H reduced by a factor (IA shown below) from typical local ISM values. Bold type indicates agreement to within a factor of 5.

Species	Observed in EC2	Model 8	Model 2	Model 9	Model 10
		$A_V = 2 \text{ mag}$ CRI = 20 × UV = 1 × IA = 0.1 ×	$A_V = 1 \text{ mag}$ CRI = 20 × UV = 1 × IA = 0.2 ×	$A_V = 1 \text{ mag}$ CRI = 20 × UV = 1 × IA = 0.4 ×	$A_V = 1 \text{ mag}$ CRI = 20 × UV = 1 × IA = 1 ×
^{13}CO	1.45e-06	3.48e-07	2.51e-07	6.36e-07	2.21e-06
C	1.04e-06	1.30e-05	1.37e-05	3.05e-05	8.90e-05
C^{18}O	1.36e-06	3.48e-07	2.51e-07	6.36e-07	2.21e-06
C_2D	<4.49e-11	3.58e-12	1.48e-11	1.22e-11	7.92e-12
C_2H	6.96e-10	1.92e-09	1.71e-08	1.99e-08	1.98e-08
CN	3.09e-11	7.89e-10	1.24e-09	3.69e-09	8.57e-09
CO	1.22e-07	3.48e-07	2.51e-07	6.36e-07	2.21e-06
CS (2–1)	4.57e-11	6.44e-11	2.87e-10	9.73e-10	3.46e-09
CS (3–2)	5.07e-12	6.44e-11	2.87e-10	9.73e-10	3.46e-09
DCN	<2.23e-11	8.97e-15	1.24e-14	2.10e-14	3.19e-14
DCO^+	<1.58e-12	3.12e-14	6.16e-15	4.19e-15	2.51e-15
H^{13}CN	<8.35e-11	6.31e-12	1.07e-11	3.04e-11	7.78e-11
H^{13}CO^+	<6.71e-11	1.06e-11	6.60e-12	6.18e-12	5.80e-12
H_2CO	7.58e-11	7.36e-11	7.70e-11	7.73e-11	6.19e-11
HC_3N	<3.54e-12	1.85e-13	7.26e-13	1.19e-12	1.24e-12
HCN	1.49e-11	6.31e-12	1.07e-11	3.04e-11	7.78e-11
HCO^+	1.96e-11	1.06e-11	6.60e-12	6.18e-12	5.80e-12
HDCO	<8.70e-13	9.07e-13	2.68e-13	1.68e-13	7.19e-14
HNC	4.70e-12	5.08e-11	2.09e-11	4.23e-11	8.88e-11
N_2H^+	<1.31e-12	4.78e-14	1.88e-14	6.39e-14	1.65e-13
NH_3	7.80e-11	6.46e-12	2.02e-13	2.80e-13	3.08e-13
SO	1.34e-10	1.35e-15	6.43e-16	1.91e-15	6.54e-15

Table 12.4: Comparison of observations of Edge Cloud 2 (EC2) with four different model predictions at steady-state, but with varying $x(\text{S})$ initial abundance. Abundances given relative to $N(\text{H}_2) = 7.4 \times 10^{22} \text{ cm}^{-2}$, with $n(\text{H}_2) = 1.2 \times 10^4 \text{ cm}^{-3}$ and $T = 20 \text{ K}$. Apart from S, most model initial abundances relative to H reduced by a factor of 5 from typical local ISM values. Bold type indicates agreement to within a factor of 5.

Species	Observed in EC2	Model 2 $A_V = 1 \text{ mag}$ $\text{CRI} = 20 \times$ $\text{UV} = 1 \times$ $x(\text{S}) = 2.0\text{e-}08$	Model 11 $A_V = 1 \text{ mag}$ $\text{CRI} = 20 \times$ $\text{UV} = 1 \times$ $x(\text{S}) = 5.0\text{e-}08$	Model 12 $A_V = 1 \text{ mag}$ $\text{CRI} = 20 \times$ $\text{UV} = 1 \times$ $x(\text{S}) = 1.0\text{e-}07$	Model 13 $A_V = 1 \text{ mag}$ $\text{CRI} = 20 \times$ $\text{UV} = 1 \times$ $x(\text{S}) = 1.0\text{e-}06$
^{13}CO	1.45e-06	2.51e-07	2.49e-07	2.46e-07	2.13e-07
C	1.04e-06	1.37e-05	1.37e-05	1.38e-05	1.42e-05
C^{18}O	1.36e-06	2.51e-07	2.49e-07	2.46e-07	2.13e-07
C_2D	<4.49e-11	1.48e-11	1.45e-11	1.40e-11	8.82e-12
C_2H	6.96e-10	1.71e-08	1.67e-08	1.61e-08	1.00e-08
CN	3.09e-11	1.24e-09	1.22e-09	1.18e-09	8.07e-10
CO	1.22e-07	2.51e-07	2.49e-07	2.46e-07	2.13e-07
CS (2–1)	4.57e-11	2.87e-10	7.00e-10	1.35e-09	8.58e-09
CS (3–2)	5.07e-12	2.87e-10	7.00e-10	1.35e-09	8.58e-09
DCN	<2.23e-11	1.24e-14	1.23e-14	1.22e-14	1.09e-14
DCO^+	<1.58e-12	6.16e-15	6.10e-15	5.99e-15	4.68e-15
H^{13}CN	<8.35e-11	1.07e-11	1.06e-11	1.05e-11	9.37e-12
H^{13}CO^+	<6.71e-11	6.60e-12	6.55e-12	6.47e-12	5.33e-12
H_2CO	7.58e-11	7.70e-11	7.67e-11	7.61e-11	7.00e-11
HC_3N	<3.54e-12	7.26e-13	7.06e-13	6.76e-13	3.68e-13
HCN	1.49e-11	1.07e-11	1.06e-11	1.05e-11	9.37e-12
HCO^+	1.96e-11	6.60e-12	6.55e-12	6.47e-12	5.33e-12
HDCO	<8.70e-13	2.68e-13	2.66e-13	2.63e-13	2.25e-13
HNC	4.70e-12	2.09e-11	2.08e-11	2.06e-11	1.88e-11
N_2H^+	<1.31e-12	1.88e-14	1.83e-14	1.77e-14	1.12e-14
NH_3	7.80e-11	2.02e-13	1.99e-13	1.94e-13	1.38e-13
SO	1.34e-10	6.43e-16	1.61e-15	3.21e-15	3.23e-14

12: CHEMICAL MODELLING OF EC2

Table 12.5: Comparison of observations of Edge Cloud 2 (EC2) with four different model predictions at steady-state, but with varying $x(\text{N})$ initial abundance. Abundances given relative to $N(\text{H}_2) = 7.4 \times 10^{22} \text{ cm}^{-2}$, with $n(\text{H}_2) = 1.2 \times 10^4 \text{ cm}^{-3}$ and $T = 20 \text{ K}$. Apart from N, most model initial abundances relative to H reduced by a factor of 5 from typical local ISM values. Bold type indicates agreement to within a factor of 5.

Species	Observed in EC2	Model 2 $A_V = 1 \text{ mag}$ $\text{CRI} = 20 \times$ $\text{UV} = 1 \times$ $x(\text{N}) =$	Model 14 $A_V = 1 \text{ mag}$ $\text{CRI} = 20 \times$ $\text{UV} = 1 \times$	Model 15 $A_V = 1 \text{ mag}$ $\text{CRI} = 20 \times$ $\text{UV} = 1 \times$	Model 16 $A_V = 1 \text{ mag}$ $\text{CRI} = 20 \times$ $\text{UV} = 1 \times$
^{13}CO	1.45e-06	2.51e-07	2.53e-07	2.55e-07	2.55e-07
C	1.04e-06	1.37e-05	1.37e-05	1.37e-05	1.37e-05
C^{18}O	1.36e-06	2.51e-07	2.53e-07	2.55e-07	2.55e-07
C_2D	<4.49e-11	1.48e-11	1.49e-11	1.50e-11	1.50e-11
C_2H	6.96e-10	1.71e-08	1.72e-08	1.73e-08	1.74e-08
CN	3.09e-11	1.24e-09	7.37e-10	1.73e-10	1.80e-11
CO	1.22e-07	2.51e-07	2.53e-07	2.55e-07	2.55e-07
CS (2–1)	4.57e-11	2.87e-10	2.89e-10	2.92e-10	2.92e-10
CS (3–2)	5.07e-12	2.87e-10	2.89e-10	2.92e-10	2.92e-10
DCN	<2.23e-11	1.24e-14	6.18e-15	1.23e-15	1.23e-16
DCO^+	<1.58e-12	6.16e-15	6.19e-15	6.21e-15	6.21e-15
H^{13}CN	<8.35e-11	1.07e-11	4.94e-12	8.98e-13	8.73e-14
H^{13}CO^+	<6.71e-11	6.60e-12	6.69e-12	6.77e-12	6.79e-12
H_2CO	7.58e-11	7.70e-11	7.71e-11	7.73e-11	7.73e-11
HC_3N	<3.54e-12	7.26e-13	3.67e-13	7.40e-14	7.41e-15
HCN	1.49e-11	1.07e-11	4.94e-12	8.98e-13	8.73e-14
HCO^+	1.96e-11	6.60e-12	6.69e-12	6.77e-12	6.79e-12
HDCO	<8.70e-13	2.68e-13	2.69e-13	2.69e-13	2.70e-13
HNC	4.70e-12	2.09e-11	9.73e-12	1.79e-12	1.74e-13
N_2H^+	<1.31e-12	1.88e-14	5.56e-15	2.61e-16	2.71e-18
NH_3	7.80e-11	2.02e-13	8.22e-14	1.22e-14	1.10e-15
SO	1.34e-10	6.43e-16	6.44e-16	6.46e-16	6.46e-16

12.3: FRACTIONAL ABUNDANCES OVER TIME

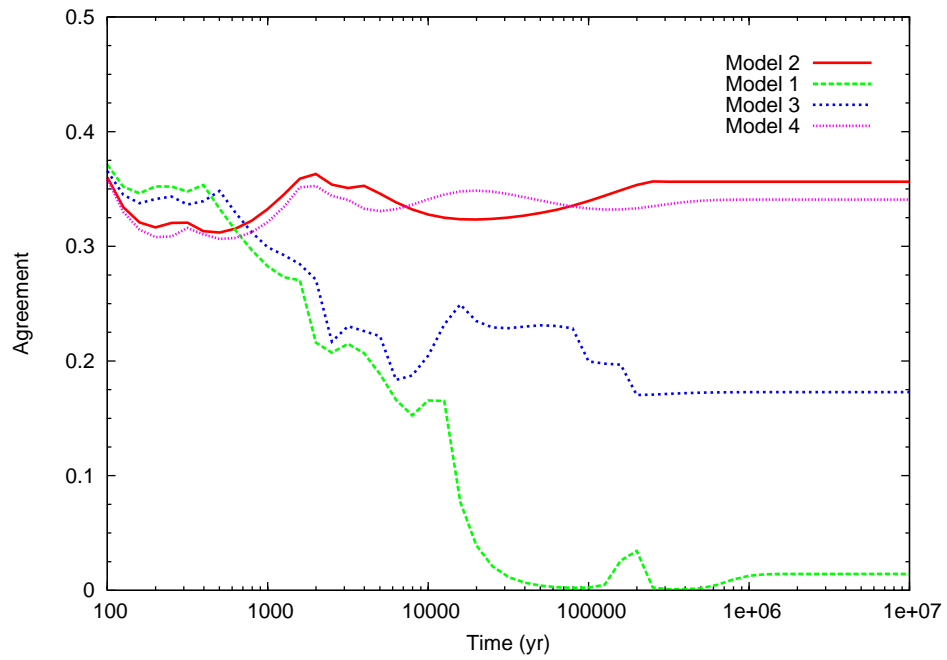


Figure 12.1: Agreement factor varying over time for Models 1–4, where A_V (mag) and cosmic ray ionisation (CRI) rates are varied (see Figs. 12.11, 12.12a and Table 12.1).

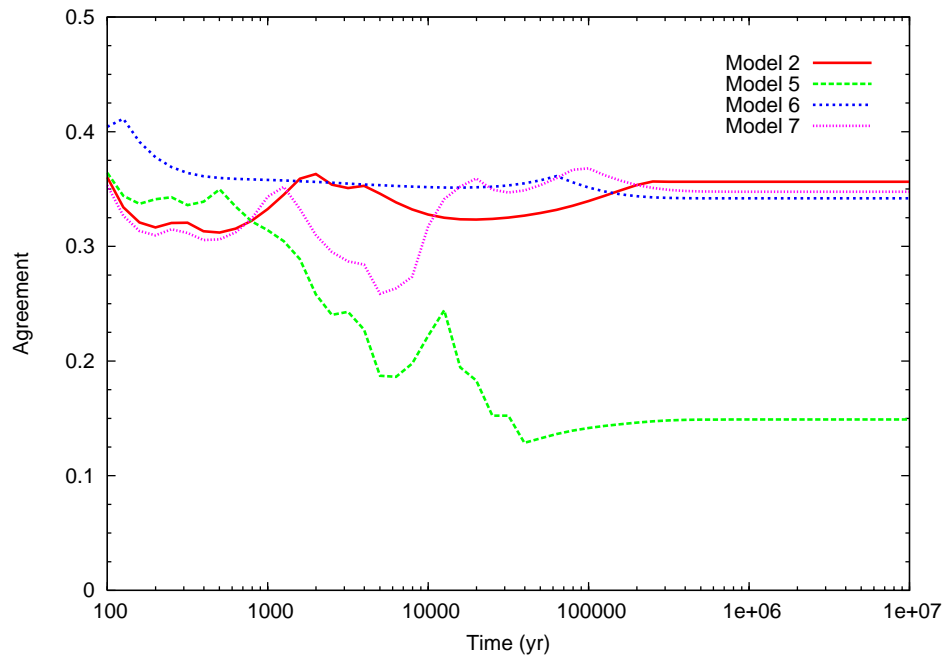


Figure 12.2: Agreement factor varying over time for Models 2, 5–7, where the UV field is varied (see Figs. 12.12b, 12.13a and Table 12.2).

12: CHEMICAL MODELLING OF EC2

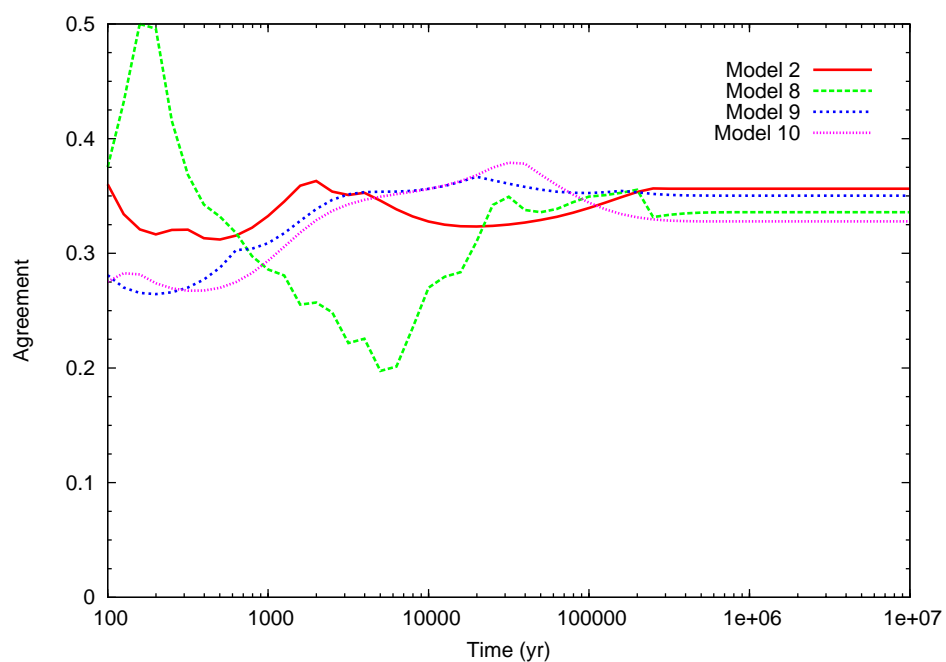


Figure 12.3: Agreement factor varying over time for Models 2, 8–10, where initial abundances are varied (see Fig. 12.13b and Table 12.3).

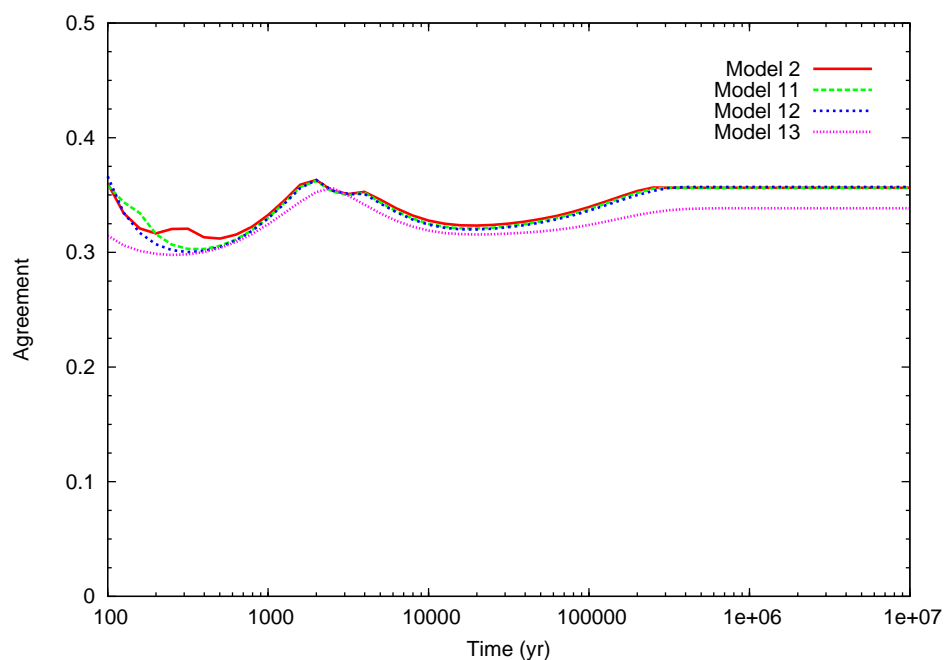


Figure 12.4: Agreement factor varying over time for Models 2, 11–13, where initial abundance of S is increased (see Fig. 12.15a and Table 12.4).

12.3: FRACTIONAL ABUNDANCES OVER TIME

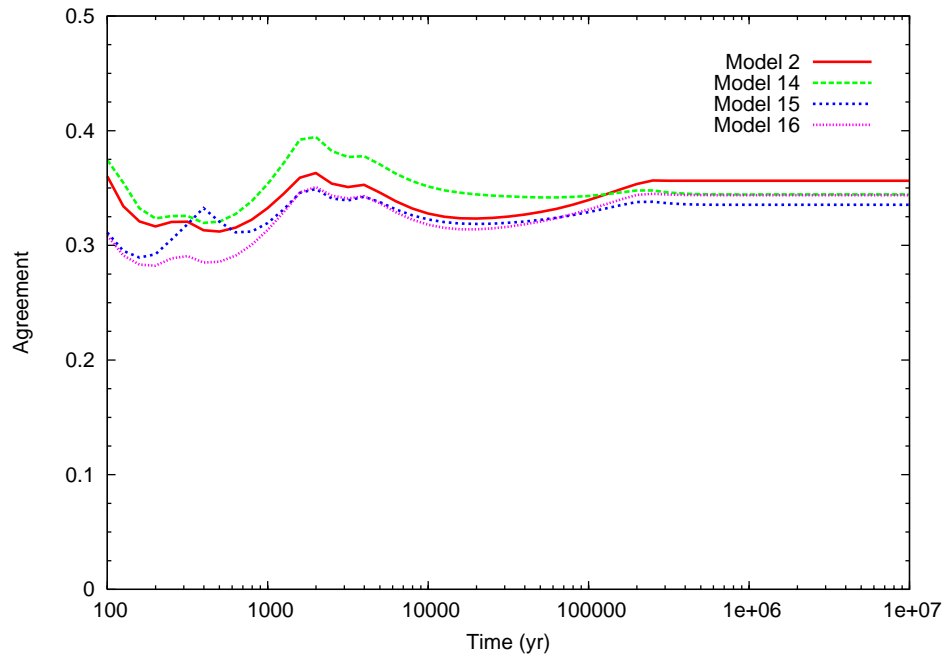


Figure 12.5: Agreement factor varying over time for Models 2, 14–16, where initial abundance of N is depleted (see Fig. 12.15b and Table 12.5).

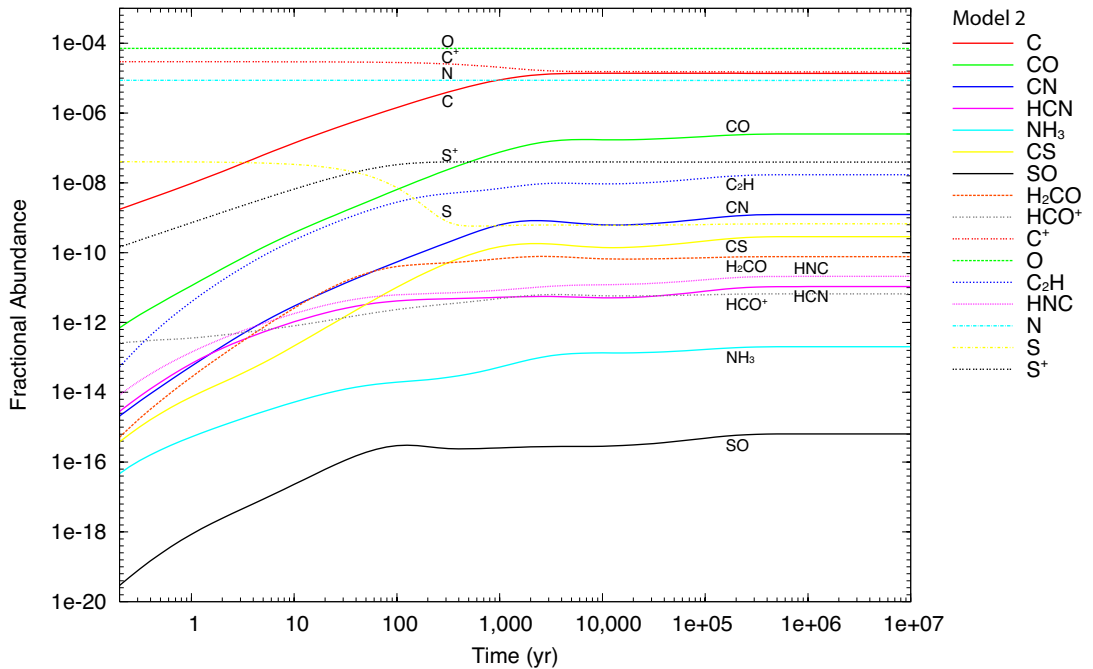


Figure 12.6: Fractional abundances varying over time for Model 2, where $A_V = 1$ mag, $\text{CRI} = 20 \times$, $\text{UV} = 1 \times$, $\text{IA} = 0.2 \times$, $n(\text{H}_2) = 1.2 \times 10^4 \text{ cm}^{-3}$, $T = 20 \text{ K}$ (see Table 12.1).

12: CHEMICAL MODELLING OF EC2

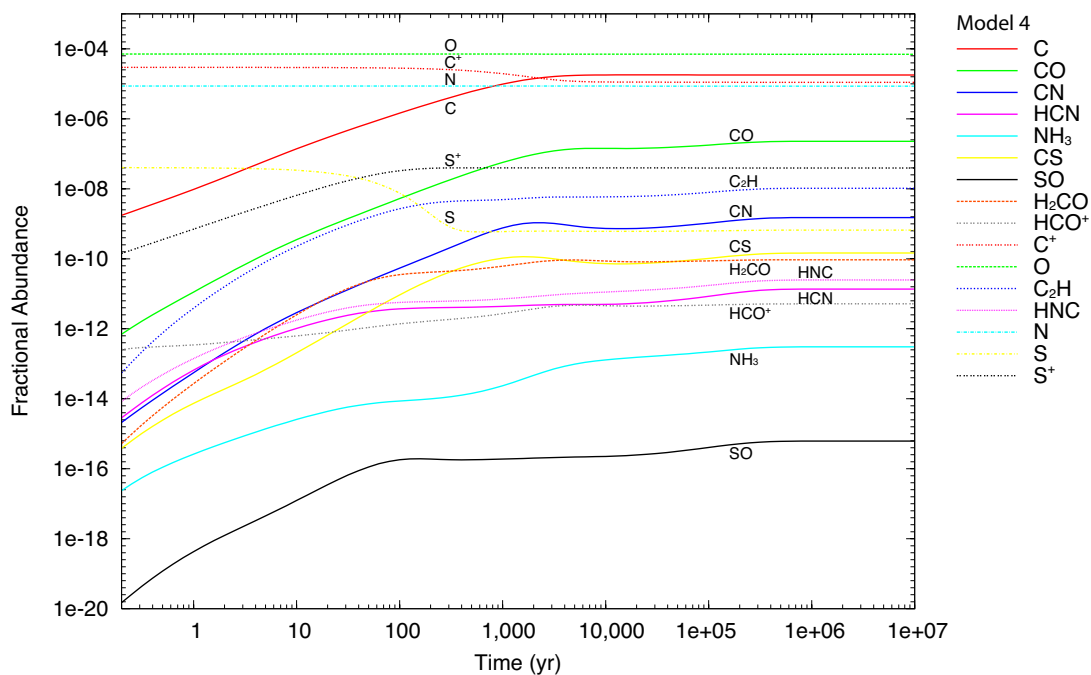


Figure 12.7: Fractional abundances varying over time for Model 4, where $A_V = 2$ mag, $\text{CRI} = 10 \times$, $\text{UV} = 10 \times$, $\text{IA} = 0.2 \times n(\text{H}_2) = 1.2 \times 10^4 \text{ cm}^{-3}$, $T = 20 \text{ K}$ (see Table 12.1).

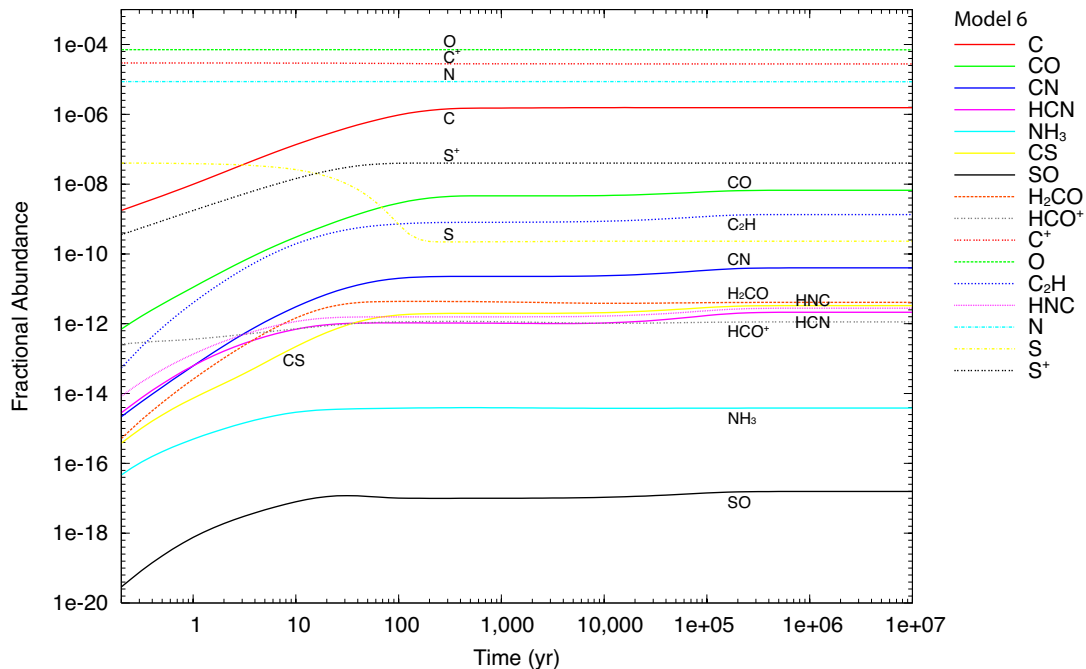


Figure 12.8: Fractional abundances varying over time for Model 6, where $A_V = 1$ mag, $\text{CRI} = 20 \times$, $\text{UV} = 20 \times$, $\text{IA} = 0.2 \times n(\text{H}_2) = 1.2 \times 10^4 \text{ cm}^{-3}$, $T = 20 \text{ K}$ (see Table 12.2).

12.3: FRACTIONAL ABUNDANCES OVER TIME

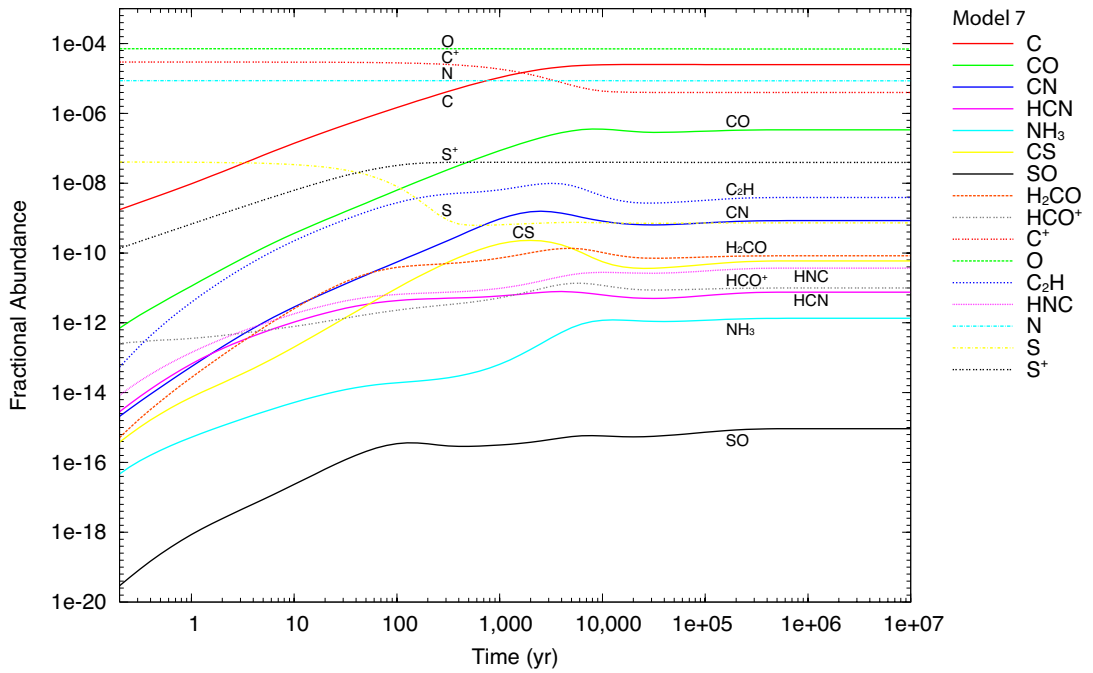


Figure 12.9: Fractional abundances varying over time for Model 7, where $A_V = 3$ mag, $\text{CRI} = 20 \times$, $\text{UV} = 40 \times$, $\text{IA} = 0.2 \times n(\text{H}_2) = 1.2 \times 10^4 \text{ cm}^{-3}$, $T = 20 \text{ K}$ (see Table 12.2).

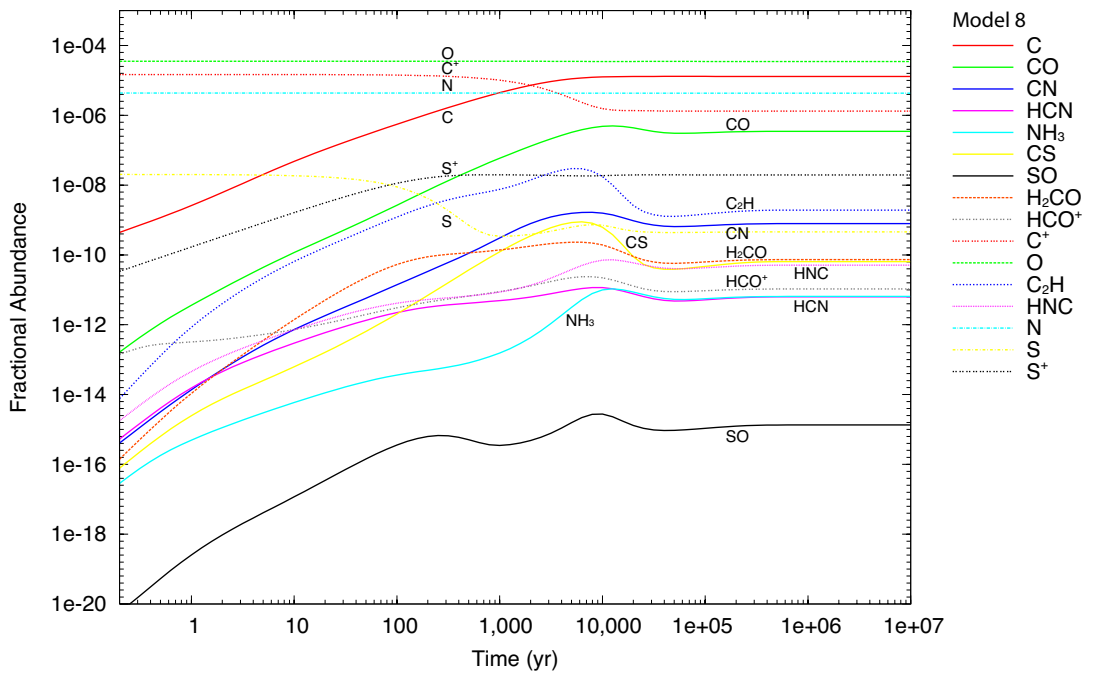


Figure 12.10: Fractional abundances varying over time for Model 8, where $A_V = 2$ mag, $\text{CRI} = 20 \times$, $\text{UV} = 1 \times$, $\text{IA} = 0.1 \times n(\text{H}_2) = 1.2 \times 10^4 \text{ cm}^{-3}$, $T = 20 \text{ K}$ (see Table 12.3).

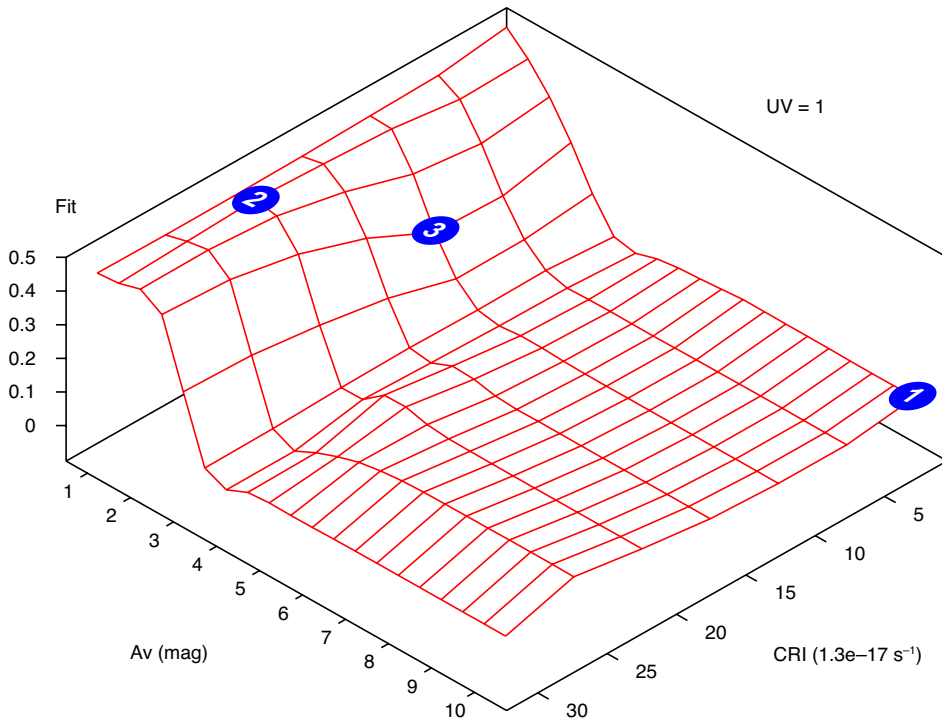


Figure 12.11: Agreement factor for models with varying A_V (mag) and cosmic ray ionisation (CRI) in terms of the standard ISM rate of $1.3 \times 10^{-17} \text{ s}^{-1}$. $T = 20 \text{ K}$, $n(\text{H}_2) = 1.2 \times 10^4 \text{ cm}^{-3}$, with a UV field set to the local ISM value, and most initial abundances reduced by a factor of 5 from typical local ISM values (see Table 12.6). Numbered blue disks indicate specific models relative to the parameter surface.

Table 12.6: Initial abundances relative to H. Most (C^+ , N, O, S, Si and Fe^+) have been reduced by a factor of 5 from those typically used to model the local ISM.

Species	Abundance	Species	Abundance
He	1.4×10^{-1}	HD	3.2×10^{-5}
C^+	1.46×10^{-5}	N	4.28×10^{-6}
O	3.51×10^{-5}	S	2.0×10^{-8}
Si	3.99×10^{-9}	Fe^+	1.99×10^{-9}

12.3: FRACTIONAL ABUNDANCES OVER TIME

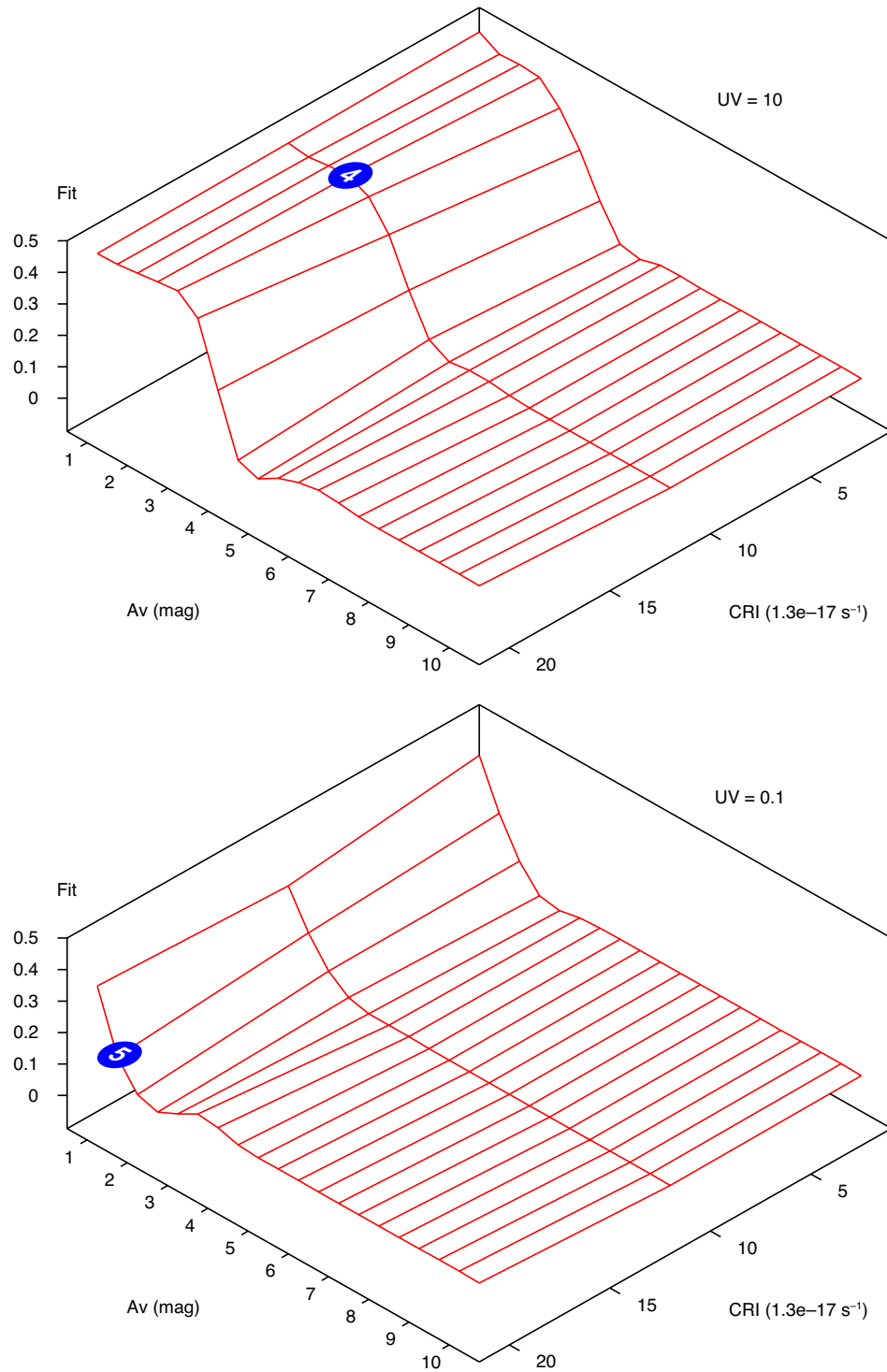


Figure 12.12: Agreement factor for models with varying A_V (mag), cosmic ray ionisation (CRI) in terms of the standard ISM rate of $1.3 \times 10^{-17} \text{ s}^{-1}$, and high or low UV field: (a) UV field increased by a factor of 10 compared to the local ISM value; (b) UV field reduced by a factor of 10 compared to the local ISM value. $T = 20 \text{ K}$, $n(\text{H}_2) = 1.2 \times 10^4 \text{ cm}^{-3}$, most initial abundances reduced by a factor of 5.

12: CHEMICAL MODELLING OF EC2

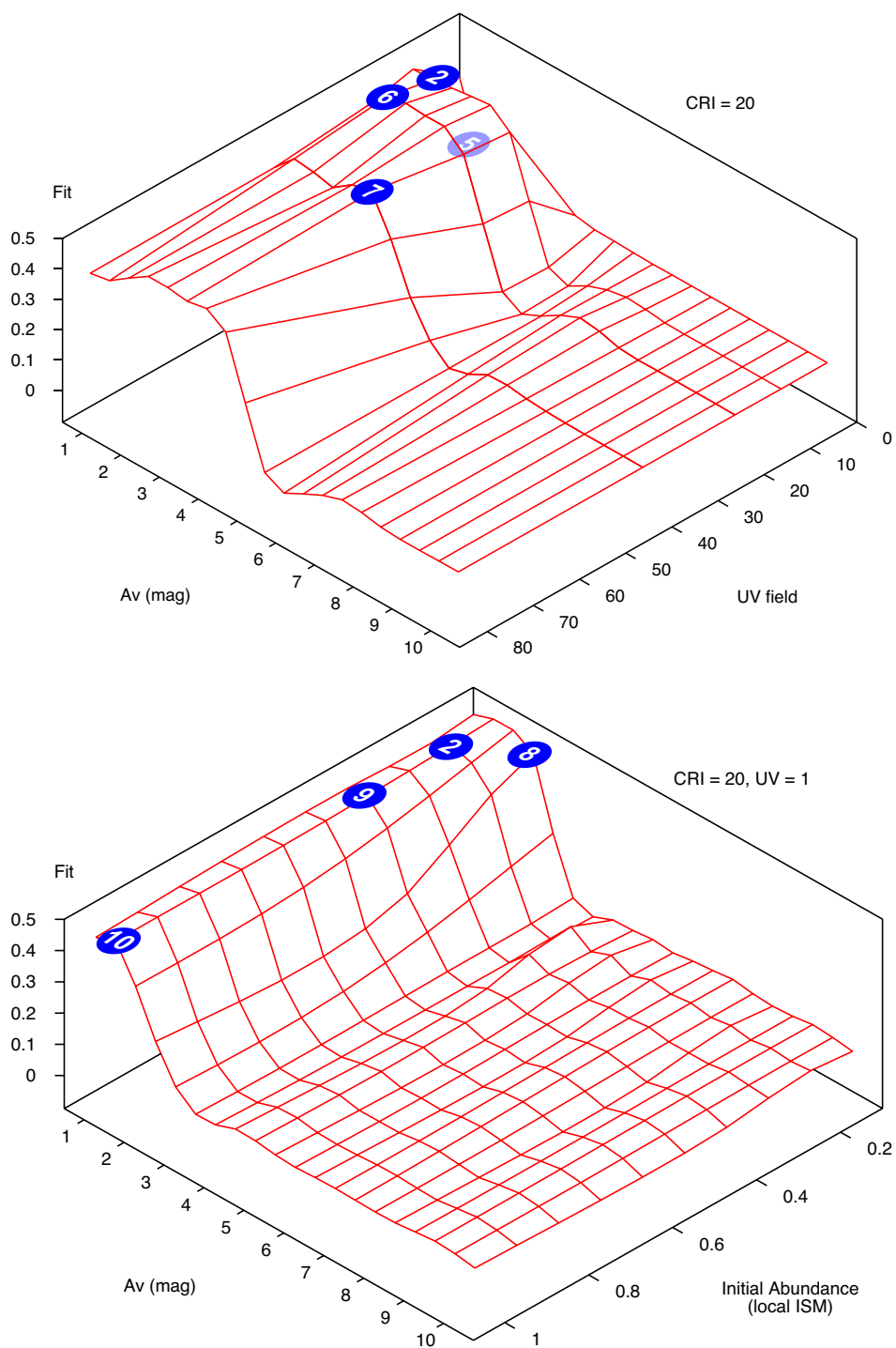


Figure 12.13: Agreement factor for models with varying A_V (mag) and: (a) an increasing UV field compared to the local ISM value, and most initial abundances reduced by a factor of 5; (b) most initial abundances reducing relative to typical local ISM values (Table 12.6), and a UV field set to the local ISM value. CRI rate = $20 \times 1.3 \times 10^{-17} \text{ s}^{-1}$, $T = 20 \text{ K}$, $n(\text{H}_2) = 1.2 \times 10^4 \text{ cm}^{-3}$.

12.3: FRACTIONAL ABUNDANCES OVER TIME

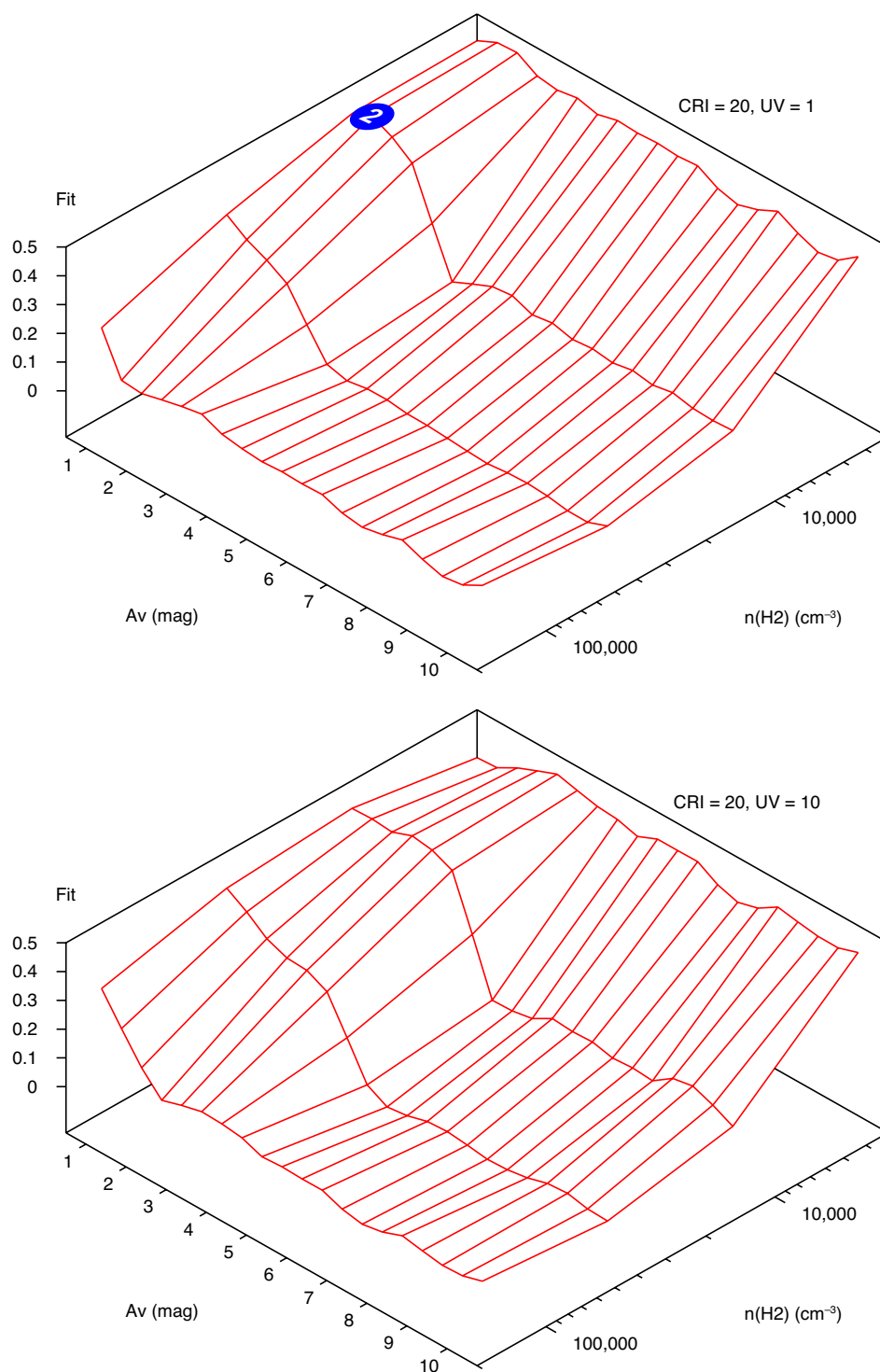


Figure 12.14: Agreement factor for models with varying A_V (mag) and $n(\text{H}_2)$ (cm^{-3}):
 (a) UV field set to the local ISM value;
 (b) UV field increased by a factor of 10 compared to the local ISM value.
 Cosmic ray ionisation (CRI) rate = $20 \times 1.3 \times 10^{-17} \text{ s}^{-1}$, $T = 20 \text{ K}$, and most initial abundances reduced by a factor of 5 (see Table 12.6).

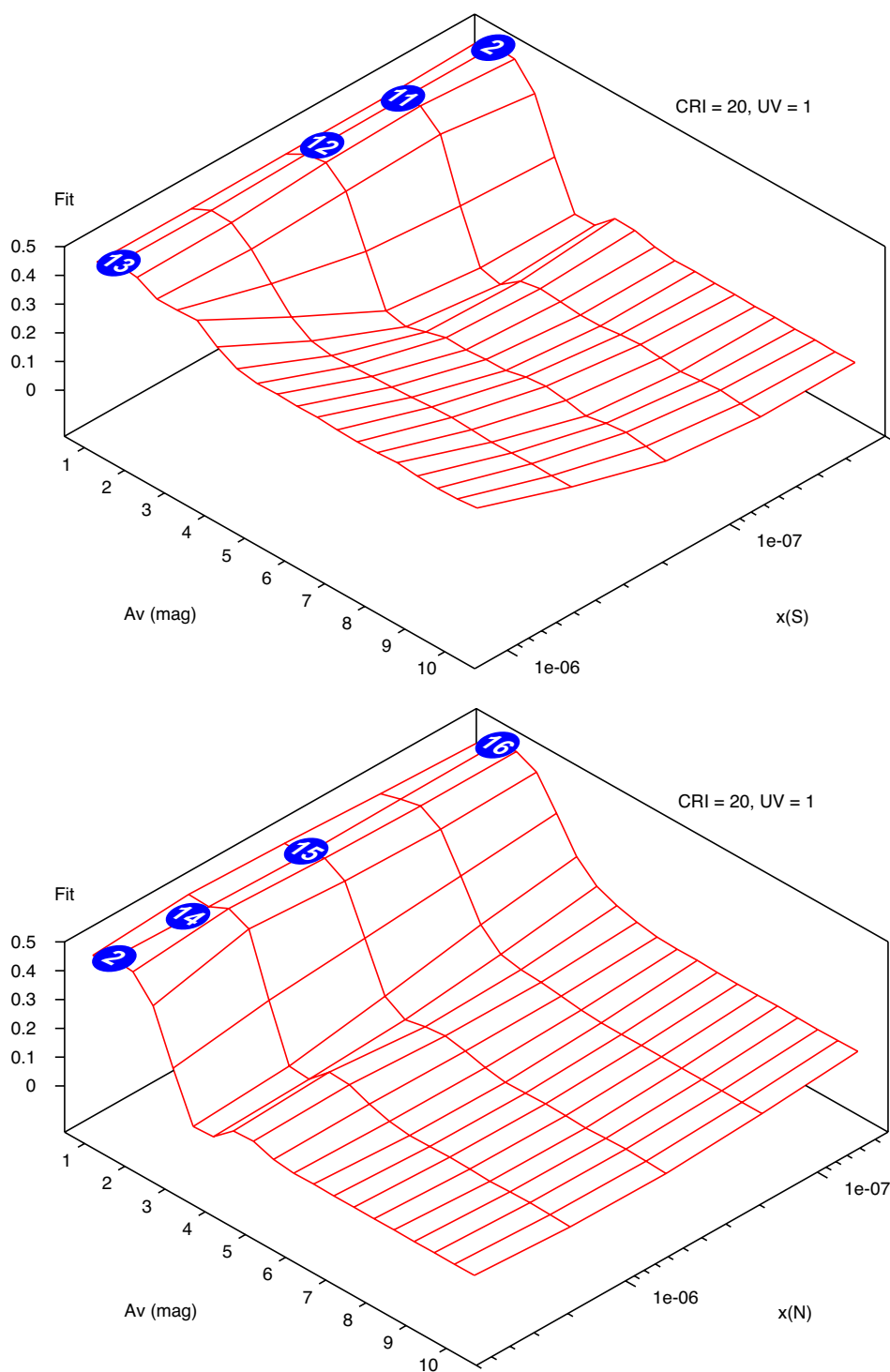


Figure 12.15: Agreement factor for models with varying A_V (mag) and initial abundances for: (a) sulphur, increasing $x(S)$; (b) nitrogen, reducing $x(N)$. Cosmic ray ionisation (CRI) rate = $20 \times 1.3 \times 10^{-17} \text{ s}^{-1}$, $T = 20 \text{ K}$, $n(\text{H}_2) = 1.2 \times 10^4 \text{ cm}^{-3}$, with a UV field set to the local ISM value, and most other initial abundances reduced by a factor of 5 (see Table 12.6).